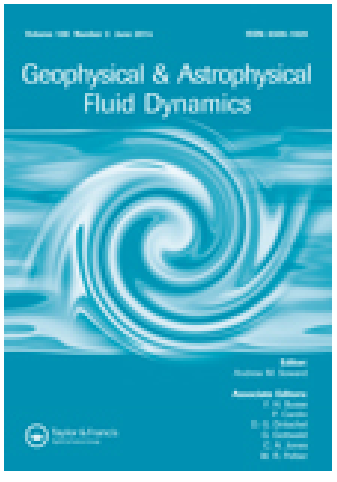

Geophysical & Astrophysical Fluid Dynamics

Publication details, including instructions for authors and subscription information:
http://www.tandfonline.com/loi/ggaf20

Rossby wave patterns in zonal and meridional winds

C.T. Duba[a], T.B. Doyle[bc] & J.F. McKenzie[a]

[a] Department of Mathematics Statistics and Physics, Durban University of Technology, P.O. Box 1334, Durban 4001, South Africa.

[b] iThemba Laboratory for Accelerator Based Sciences, Somerset West 7129, South Africa.

[c] School of Chemistry and Physics, University of KwaZulu-Natal, Westville, South Africa.

Published online: 31 Mar 2014.

To cite this article: C.T. Duba, T.B. Doyle & J.F. McKenzie (2014) Rossby wave patterns in zonal and meridional winds, Geophysical & Astrophysical Fluid Dynamics, 108:3, 237-257, DOI: 10.1080/03091929.2013.867604

To link to this article: http://dx.doi.org/10.1080/03091929.2013.867604

Geophysical and Astrophysical Fluid Dynamics, 2014
Vol. 108, No. 3, 237–257, http://dx.doi.org/10.1080/03091929.2013.867604

Rossby wave patterns in zonal and meridional winds

C.T. DUBA*†, T.B. DOYLE‡§ and J.F. MCKENZIE†

†Department of Mathematics Statistics and Physics, Durban University of Technology, P.O. Box 1334, Durban 4001, South Africa
‡iThemba Laboratory for Accelerator Based Sciences, Somerset West 7129, South Africa
§School of Chemistry and Physics, University of KwaZulu-Natal, Westville, South Africa

(*Received 15 July 2013; in final form 15 November 2013; first published online 31 March 2014*)

The propagation properties of Rossby waves in zonal and meridional winds are analyzed using the local dispersion relation in its wave number form, the geometry of which plays a crucial role in illuminating radiation patterns and ray trajectories. In the presence of a wind/current, the classical Rossby wave number curve, an offset circle, is distorted by the Doppler shift in frequency and a new branch, consisting of a blocking line with an eastward facing indentation, arises from waves convected with or against the flow. The radiation patterns generated by a time harmonic compact source in the laboratory frame are calculated using the method of stationary phase and are illustrated through a series of figures given by the reciprocal polars to the various types of wave number curves. We believe these results are new. Some of these wave patterns are reminiscent of a "reversed" ship wave pattern in which cusps (caustics) arise from the points of inflection of the wave number curves; whilst others bear a resemblance to the parabolic like curves characteristic of the capillary wave pattern formed around an obstacle in a stream. The Rossby stationary wave in a westerly is similar to the gravity wave pattern in a wind, whereas its counterpart in a meridional wind exhibits caustics, again arising from points of inflection in the wavenumber curve.

Keywords: Rossby waves; β-plane; Radiation pattern

1. Introduction

Rossby waves play a pivotal role in the transport of energy and momentum in the geophysical fluid dynamics of quasi-geostrophic flows in atmospheres and oceans. The particular wave dynamics arise from the latitudinal variation of the Coriolis acceleration (through the Coriolis parameter f) and the near balance achieved between it and the pressure gradient. This quasi-geostrophic balance is described within the framework of the β-plane approximation which retains the essential dynamics, whilst the spherical geometry is replaced with a Cartesian β-plane constructed tangential to the surface at a given latitude. These features have all been extensively discussed in the texts of Gill (1982), Pedlosky (1987), Vallis (2006), and elsewhere. Some of the latter will be referenced to in the following.

In this well-researched field it may be expected that there is nothing new or interesting to reveal about the linear behavior of Rossby waves. However, recently it has been shown

*Corresponding author. Email: thamadub@dut.ac.za

that the group velocity diagram, at a given wave frequency, is in fact an ellipse whose focus lies at the origin (Duba and McKenzie 2012, McKenzie under review). This elegant feature complements the wave number curve, namely an offset circle in wave number space (Longuet-Higgins 1964), in revealing the propagation properties of Rossby waves. Furthermore, it has been shown (Rhines 2003, McKenzie under review) that the radiation pattern of Rossby waves (in the wind-free case) consists of two sets of hyperbolae, confined to westward pointing Mach–Froude like lines, in a fashion analogous to the gravity-capillary waves generated by an obstacle in uniform motion on deep water (see Doyle and McKenzie (2013) for a recent treatment of this classical ship wave problem). These features of the radiation pattern generated by some time harmonic spatially compact source are illuminated by the use of the method of stationary phase in calculating the far field disturbance. This method demonstrates that the radiation pattern is in fact given by the reciprocal polar to the wave normal curve (Lighthill 1978, 1960, p. 372–373) and this simple geometrical construction provides not only the mathematical expressions for, but also a means of visualizing, the radiation pattern which, in zonal and meridional winds reveals new and interesting patterns.

In this paper, we extend the above analysis to include the effects of zonal and meridional winds which give rise to new and interesting features of the wave number curves resulting from the Doppler shift in frequency. In a recent paper, Gerkema *et al.* (2013) call this effect a "quasi-Doppler shift" referring to the difference between the frequency ω measured by an observer at rest (the laboratory frame) and the frequency $\hat{\omega}$ measured by an observer moving with the mean flow. This shift has a profound effect on wave propagation in a moving medium, particularly if the medium is both dispersive and anisotropic, as is indeed the case for Rossby waves. The wave number diagrams therefore are important in revealing the propagation properties of Rossby waves, in much the same way as the Appleton–Hartree refractive index (Ratcliffe 1972, p. 18, section 2.5) is crucial to the understanding of electromagnetic waves in a magneto-ionic medium, and of the slowness ($\boldsymbol{k}$) surfaces in MHD (Lighthill 1960).

In section 2, we develop the standard equations of motion on a β-plane and derive the wave energy equation. Although the Coriolis term makes no contribution to this equation, it nevertheless has an indirect effect through shaping the propagation properties of the natural modes (inertial and planetary) of the system. In section 3, we derive the coupled equations for the northward and eastward mass flux perturbations and the excess pressure (all of which are shown to be equivalent to the shallow water equations with an appropriate definition of the Kelvin speed). In the case of Fourier type zonal wave modes, the coupled equations reduce to a single second-order differential equation for the latitudinal structure of the northward mass flux.

In section 4, we examine the wave propagation properties revealed by the dispersion equation in the form of wave number curves at a given frequency ω in the laboratory frame for different values of the zonal and meridional wind speeds. These diagrams enable the calculation of the radiation pattern generated by a time harmonic spatially compact source in a steady, uniform wind, through the reciprocal polar to the appropriate wave number curve. For example, in the case of a westerly zonal wind, its effect is to distort the Longuet-Higgins circle into an ovoid-shaped curve, and importantly, to introduce a new branch, due to the Doppler shift, consisting essentially of a blocking line with an indentation to the right (i.e. eastward) of this line, and corresponds to propagation arising from waves convected with or against the zonal flow. The reciprocal polar of the (closed) ovoid curve is a parabolic like curve corresponding to both eastward and westward energy propagation; whilst that for the line with an indentation we have an eastward facing deltoid, reminiscent of an inverted or "reversed" Kelvin ship wave. In this case, the radiation pattern is confined to a Kelvin-like angle (given by a line drawn from the

origin to the cusp point which arises from the point of inflection in the wave number curve). The analysis for westward zonal flow (an easterly) reveals similar features with a parabolic like curve for the reciprocal polar within which is embedded a Kelvin-like ship wave deltoid facing the "correct" way (i.e. eastward) associated with the indented line. An analysis of the effects of a meridional wind, including the stationary wave patterns (obtained as the limit in which the frequency ω tends to zero) yields similar interesting features but with the presence of a north-south symmetry.

2. Linearized equations of motion in a zonal wind shear

The linearized continuity equation is given by

$$\frac{\mathrm{D}\rho_e}{\mathrm{D}t} + \nabla \cdot \boldsymbol{q} = 0, \tag{1}$$

in which $\mathrm{D}/\mathrm{D}t = \partial/\partial t + U_x(y)\partial/\partial x$ is the convective derivative, $\boldsymbol{q} = \rho_0 \boldsymbol{u}$ is the mass flux perturbation, where ρ_0 is the background density, $\boldsymbol{u}$ is the velocity perturbation, ρ_e is the density perturbation, and $U_x(y)$ is a given zonal flow sheared in the y (north) direction. The x (east), y (north), and z (vertical) components of the momentum equation are

$$\frac{\mathrm{D}q_x}{\mathrm{D}t} - (f - U')q_y = -\frac{\partial p_e}{\partial x}, \tag{2a}$$

$$\frac{\mathrm{D}q_y}{\mathrm{D}t} + f q_x = -\frac{\partial p_e}{\partial y}, \tag{2b}$$

$$\frac{\mathrm{D}q_z}{\mathrm{D}t} = -\frac{\partial p_e}{\partial z} - \rho_e g, \tag{2c}$$

respectively, in which p_e is the pressure perturbation and U' is the derivative of $U_x(y)$ with respect to y. We have assumed a β-plane approximation, at a given latitude θ_0 on a planet with radius R. Ω is the earth's rotation frequency, so that the Coriolis parameter f is given by

$$f = f_0 + \beta y, \qquad \beta_0 = \frac{2\Omega}{R}\cos\theta_0. \tag{3a,b}$$

The equation for adiabatic flow (which, in the dissipationless case, is equivalent to the energy equation) takes the form (Lighthill 1978, p. 292, section 4.2)

$$g\frac{\mathrm{D}\rho_e}{\mathrm{D}t} = N^2 q_z + \frac{g}{c_0^2}\frac{\mathrm{D}p_e}{\mathrm{D}t}, \tag{4}$$

in which the square of the Brunt–Väisälä frequency N is given by

$$N^2 = g\left(-\frac{1}{\rho_0}\frac{\mathrm{d}\rho_0}{\mathrm{d}z} - \frac{g}{c^2}\right) = (g/H)(1 - \gamma^{-1}), \tag{5}$$

where H is the density scale height, γ is the ratio of the specific heats, and c_0 is the speed of sound given by $\sqrt{\gamma p_0/\rho_0}$. The background state is described by hydrostatic equilibrium and geostrophic balance, namely

$$\frac{\partial p_0}{\partial z} = -\rho_0 g, \qquad \frac{\partial p_0}{\partial y} = -\rho_0 f U_x(y). \tag{6a,b}$$

In general, these equations must be supplemented by a background energy equation which includes heating, cooling, and dissipation processes such as those resulting from viscous and heat conduction effects, in order to completely determine the background state (ρ_0, p_0, U_x).

The perturbation equations (1), (2), and (4) can be somewhat simplified by using the Boussinesq approximation which filters out high frequency acoustic waves. This is accomplished by neglecting $\mathrm{D}\rho_e/\mathrm{D}t$ in (1) which becomes

$$\nabla \cdot \boldsymbol{q} = 0, \tag{7}$$

and also by letting $c_0 \to \infty$ in the second term on the right-hand side of (4) which becomes

$$g\frac{\mathrm{D}\rho_e}{\mathrm{D}t} = N^2 q_z. \tag{8}$$

We note that in this approximation the continuity equation no longer evolves the density in time which is now evolved by the incompressible form, equation (8), for adiabatic flow, with the implication that there is now no equation which evolves the pressure. However, we note that, if we do the operation $\mathrm{D}/\mathrm{D}t$ on (2c), we obtain

$$\frac{\mathrm{D}}{\mathrm{D}t}\left(\frac{\partial p_e}{\partial z}\right) = -\frac{\mathrm{D}^2}{\mathrm{D}t^2}q_z - g\frac{\mathrm{D}\rho_e}{\mathrm{D}t}, \tag{9a}$$

$$= -\left(\frac{\mathrm{D}^2}{\mathrm{D}t^2} + N^2\right)q_z. \tag{9b}$$

The last result follows from the use of (8) to eliminate ρ_e. Furthermore, if we do the operation $\partial/\partial z$ on (9b) and use continuity in its incompressible form (7) to eliminate $\partial q_z/\partial z$, we obtain

$$\frac{\mathrm{D}}{\mathrm{D}t}\left(\frac{\partial^2 p_e}{\partial z^2}\right) = \left(\frac{\mathrm{D}^2}{\mathrm{D}t^2} + N^2\right)\left(\frac{\partial q_x}{\partial x} + \frac{\partial q_y}{\partial y}\right). \tag{10}$$

In what follows we will use the low frequency approximation $\mathrm{D}^2/\mathrm{D}t^2 \ll N^2$ (which filters out higher frequency internal gravity waves with $\omega \sim N$) and assume waves of the form $\exp(-\mathrm{i}k_z z)$ in the vertical direction, so that (10) may be written

$$\frac{\mathrm{D}p_e}{\mathrm{D}t} = -c^2\left(\frac{\partial q_x}{\partial x} + \frac{\partial q_y}{\partial y}\right), \qquad c^2 \equiv N^2/k_z^2. \tag{11a,b}$$

Here, c may be called the effective Kelvin speed which, in shallow water theory, is $\sqrt{gH}$, where H is the depth. In this rather circuitous route, we now have an equation (11a) which evolves the perturbation pressure p_e. Hence, the system has been reduced to three "evolutionary" equations, namely equations (2a,b) which evolve the horizontal components of the mass flux (or velocity) in time and (11a) which evolves p_e. These are equivalent to the shallow water equations in which the speed $c(\equiv N/k_z)$ replaces $\sqrt{gH}$, as already noted.

The system of equations, (1), (2), (4), and (8), possesses a wave energy equation which follows by taking the scalar product of the momentum equation with $\boldsymbol{q}$ to obtain

$$\frac{\mathrm{D}}{\mathrm{D}t}\left[\frac{1}{2}\left({q_x}^2 + {q_y}^2 + {q_z}^2\right)\right] + U' q_x q_y = -\boldsymbol{q}\cdot\nabla p_e - q_z\rho_e g. \tag{12}$$

The terms on the right-hand side may be written in the form

$$-\boldsymbol{q}\cdot\nabla p_e = -\nabla\cdot(p_e\boldsymbol{q}), \tag{13}$$

on using $\nabla\cdot\boldsymbol{q} = 0$, and

$$-gq_z\rho_e = -\frac{g^2}{N^2}\frac{\mathrm{D}}{\mathrm{D}t}({\rho_e}^2/2), \tag{14}$$

on using (8). Hence (12), after division through by ρ_0, assumes the "conservation form" with "sources"

$$\frac{\mathrm{D}}{\mathrm{D}t}\left[\frac{1}{2}\rho_0 u^2 + \frac{1}{2}\frac{g^2}{N^2}\frac{{\rho_e}^2}{\rho_0}\right] + \nabla\cdot(p_e\boldsymbol{u}) = -p_e u_z\left(\frac{1}{\rho_0}\frac{\mathrm{d}\rho_0}{\mathrm{d}z}\right) - \frac{\mathrm{d}U_x}{\mathrm{d}y}u_x u_y. \tag{15}$$

On the left-hand side, the first term is the rate of change of the energy density consisting of the kinetic energy and the thermobaric potential energy (Eckart 1960), and the second term is the divergence of wave energy flux. The "source" terms on the right-hand side represent wave interaction with the background state through buoyancy (the first term) and shear flow (the second term). The latter term can lead to Kelvin-Helmholtz, baroclinic type, instability, whereas the former can generate convective instability if the atmosphere is unstably stratified, $N^2 < 0$. Here we assume $N^2 > 0$.

3. The latitudinal structure equation

In this section we derive the second-order differential equation for the northward mass flux to which the zonal mass flux and pressure are related through equations (see below). Its hydromagnetic version including magnetic as well as velocity shear has been discussed by Eltayeb and McKenzie (1977) and Mekki and McKenzie (1977). Here, we examine in detail the effects of the wind, through the Doppler shift, on the propagation properties.

For Fourier wave modes of the form

$$(q_x, q_y, p_e) = (Q_x(y), Q_y(y), P_e(y))\exp\left[\mathrm{i}(\omega t - k_x x - k_z z)\right],$$

equations (2a,b) become

$$\mathrm{i}\hat{\omega}Q_x - (f - U')Q_y = \mathrm{i}k_x P_e, \tag{16a}$$

and

$$\mathrm{i}\hat{\omega}Q_y + fQ_x = -\frac{\partial P_e}{\partial y}, \tag{16b}$$

whilst (11a) reduces to

$$P_e = \frac{c^2}{\hat{\omega}}\left(k_x Q_x + \mathrm{i}\frac{\mathrm{d}Q_y}{\mathrm{d}y}\right). \tag{17}$$

Here $\hat{\omega}$ is the Doppler shifted frequency given by

$$\hat{\omega} = \omega - k_x U. \tag{18}$$

Eliminating P_e from equations (16a,b) using (17) yields the coupled system for Q_x and Q_y:

$$(\hat{\omega}^2 - {k_x}^2 c^2)Q_x = \mathrm{i}\left[k_x c^2\frac{\mathrm{d}Q_y}{\mathrm{d}y} - (f - U')\hat{\omega}Q_y\right], \tag{19a}$$

$$\hat{\omega}^2 Q_y + \hat{\omega}\frac{\mathrm{d}}{\mathrm{d}y}\left(\frac{c^2}{\hat{\omega}}\frac{\mathrm{d}Q_y}{\mathrm{d}y}\right) = \mathrm{i}\left[\hat{\omega}k_x c^2\frac{\mathrm{d}}{\mathrm{d}y}\left(\frac{Q_x}{\hat{\omega}}\right) + f\hat{\omega}Q_x\right]. \tag{19b}$$

Elimination of Q_x in (19b), using (19a), gives the second order differential equation for the latitudinal structure of $Q_y(y)$:

$$\frac{\mathrm{d}^2 Q_y}{\mathrm{d}y^2} - \left[\frac{\mathrm{d}}{\mathrm{d}y}\ln\left(\hat{\omega}^2 - c^2 k_x^2\right)\right]\frac{\mathrm{d}Q_y}{\mathrm{d}y} + \kappa^2 Q_y = 0, \tag{20a}$$

$$\kappa^2 \equiv \frac{\hat{\omega}^2 - f\left(f - U^{'}\right)}{c^2} + k_x(f - U')\frac{\mathrm{d}}{\mathrm{d}y}\ln\left(\hat{\omega}^2 - c^2k_x^2\right) - {k_x}^2 - \frac{\left(\beta - U^{''}\right)k_x}{\hat{\omega}}, \quad (20b)$$

in which we have used $\mathrm{d}f/\mathrm{d}y = \beta$, $\mathrm{d}\hat{\omega}/\mathrm{d}y = -k_x U^{'}$. At this stage the latitudinal wave number κ^2 (given by (20b)) describes gravity-inertial waves (the first term of left-hand side of (20b) and Rossby waves (the last two terms) in the presence of a zonal shear (the middle term). Equation (20) yields an invariant (related to the Wronskian) by multiplying it by ${Q_y}^*$, and its complex conjugate form by Q_y, to obtain

$$\mathrm{Im}\left\{\frac{\left({Q_y}^*\mathrm{d}Q_y/\mathrm{d}y - Q_y\mathrm{d}{Q_y}^*/\mathrm{d}y\right)}{\left(\hat{\omega}^2 - {k_x}^2c^2\right)}\right\} = \text{const.} \quad (21)$$

From the viewpoint of wave dynamics this quantity is related to the conservation of wave action except at critical points where it undergoes a discontinuous jump (Booker and Bretherton 1967, Dickinson 1968).

The connection to the classical Rossby wave latitudinal structure equation is obtained in the limit $c \to \infty$ in which (20a) reduces to

$$\frac{\mathrm{d}^2Q_y}{\mathrm{d}y^2} + \left(-{k_x}^2 - \frac{(\beta - U^{''})k_x}{\hat{\omega}}\right)Q_y = 0. \quad (22)$$

In the slowly varying (JWKB) approximation, this yields the local Rossby wave dispersion equation for k_y, namely

$${k_y}^2 + {k_x}^2 = -\beta_e\frac{k_x}{\hat{\omega}}, \quad (23a)$$

where

$$\beta_e \equiv \beta - U^{''} = \frac{\mathrm{d}}{\mathrm{d}y}\left(f - U^{'}\right). \quad (23b)$$

These results follow directly from equations (2a,b), the z component of the curl of which yields

$$\frac{\mathrm{D}}{\mathrm{D}t}\left(\frac{\partial q_y}{\partial x} - \frac{\partial q_x}{\partial y}\right) + \left(\beta - U^{''}\right)q_y = 0, \quad (24)$$

since as $c \to \infty$ we have the 2-D incompressibility equation

$$\frac{\partial q_y}{\partial y} + \frac{\partial q_x}{\partial x} = 0. \quad (25)$$

The operation $\partial/\partial x$ of (24) and the use of 2-D incompressibility condition (25) to eliminate q_x, yield the classical Rossby wave equation (for infinite Rossby radius), namely

$$\frac{\mathrm{D}}{\mathrm{D}t}\left(\frac{\partial^2 q_y}{\partial x^2} + \frac{\partial^2 q_y}{\partial y^2}\right) + (\beta - U^{''})\frac{\partial q_y}{\partial x} = 0. \quad (26)$$

For Fourier wave modes $\propto Q_y(y)\exp\mathrm{i}(\omega t - k_x x)$ this yields (22) for the latitudinal structure, in agreement with the limit obtained from our more general analysis in which $c \neq \infty$.

This last result (26) and (24) essentially express conservation of total (planetary plus zonal shear plus wave) vorticity. At the outset one could choose a derivation with the idea of using conservation of potential vorticity for a shallow layer, which would involve taking the curl of the horizontal components of the equation of motion (to give $(\nabla \times \boldsymbol{u})_z$), but this would still be coupled to an equation for the horizontal divergence, and together with suitable approximations as given above, would lead to the Potential-Vorticity equation (Rhines 2003).

4. Radiation pattern in a wind

In this section, the radiation pattern generated by a time harmonic spatially compact source in a uniform wind is analyzed. This is equivalent to calculating wave generation by traveling forcing effects (Lighthill 1960). The effects of the frequency Doppler shift play an important role in wave propagation in a moving medium. This is revealed through the geometry of the wave number curves in the laboratory frame, which in turn determine the radiation pattern using the method of stationary phase. For uniform winds, $\boldsymbol{U}$, the local dispersion equation is given by (20b), which, with derivatives of $\boldsymbol{U}$ put to zero and $\hat{\omega} \ll f$, simplifies to

$$k_y^2 + k_x^2 + f^2/c^2 = -\frac{\beta k_x}{\omega - \boldsymbol{k} \cdot \boldsymbol{U}}. \tag{27}$$

The quantity $\hat{\omega} = \omega - \boldsymbol{k} \cdot \boldsymbol{U}$ is sometimes referred to as the "intrinsic" frequency (Bretherton and Garrett 1968, Dickinson 1968, Lighthill 1978), and where it is zero the wave is said to exhibit critical level behavior (Booker and Bretherton 1967). At such a level the wave action undergoes a discontinuous jump.

4.1. *Method of stationary phase*

Asymptotic approximations to Fourier integrals, representing the solution of linear wave problems, can be evaluated by the method of stationary phase (for a detailed account, see for example, Lighthill's classical book "Waves in Fluids" 1978, p. 351–361). In the far, or radiation, field the dominant contribution to a Fourier integral, representing the solution of the problem, comes from those portions of the rapidly oscillating phase which are stationary with respect to the component of the wave number over which the integration is being carried out. For example, in the case of a two-dimensional problem such as on a β-plane, the phase $\Phi(\boldsymbol{x}, \boldsymbol{k})$ may be written, in Cartesian co-ordinates, in the form

$$\Phi = \omega t - k_x x - k_y y, \tag{28}$$

in which ω is the (given) angular frequency of the source, and $\boldsymbol{k} = (k_x, k_y)$ is the two-dimensional wave number vector. These quantities are related through a dispersion relation (for example (27) above) arising from the Fourier image of the wave operator which appears as a simple pole, thus through the calculus of residues, reducing the two-dimensional Fourier integral to a single integral over either (k_x, k_y) space (using the residue theorem), and is given by some relation

$$D(\omega - \boldsymbol{k} \cdot \boldsymbol{U}, k_x, k_y) = 0. \tag{29}$$

Here D is an algebraic function representing the Fourier image of the wave operator in which the Doppler shifted frequency $\hat{\omega} = \omega - \boldsymbol{k} \cdot \boldsymbol{U}$ arises from winds or flows of velocity $\boldsymbol{U}$ relative to the laboratory frame. This relation can be written in the polar form

$$D(\omega - kU\cos(\theta - \alpha), k, \theta) = 0 \tag{30}$$

in which $\boldsymbol{k} = k(\cos\theta, \sin\theta)$, $\boldsymbol{U} = U(\cos\alpha, \sin\alpha)$, and may have solutions

$$k(\theta) = k_i(\theta, \omega, \alpha, U), \tag{31}$$

where $i = 1, 2, \ldots, n$ represents the possible n roots of the dispersion equation representing different modes of propagation. We refer to the solutions $k_i(\theta)$ as the polar form of the wave

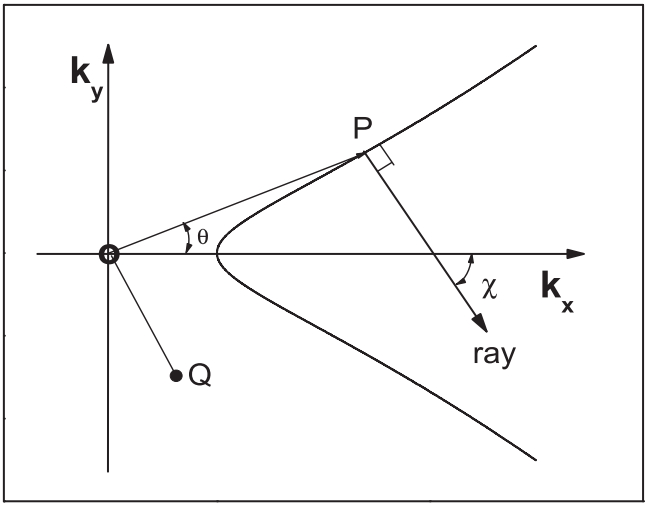

Figure 1. The geometrical interpretation of the reciprocal polar of the wave number curve. The example shown is actually appropriate to the wave number $k(\theta)$ for stationary waves on deep water ($k(\theta) \sim 1/\cos^2\theta$) generated by a uniformly moving source (ship).

number diagrams at given values of (ω, α, U) in the laboratory frame. Writing the space coordinates (x, y) in polar form $r(\cos\chi, \sin\chi)$, the phase given by (28) of the ith mode may be written

$$\Phi_i = r(\chi)k_i(\theta)\cos(\theta - \chi), \tag{32}$$

where we now regard θ, the wave number angle, as the variable over which the Fourier integral is taken. For large r (i.e. the far field) the phase Φ_i is stationary with respect to θ if

$$\frac{\partial \Phi_i}{\partial \theta} = 0, \tag{33}$$

which implies

$$\frac{k_i'(\theta)}{k_i(\theta)} = \tan(\theta - \chi), \tag{34}$$

or

$$\tan\chi = \frac{\tan\theta - (k'/k)_i}{1 + \tan\theta(k'/k)_i} = -\frac{1}{\partial k_y/\partial k_x}, \tag{35}$$

which defines the ray direction χ in terms of θ.

The radiation pattern is given by (32) which for a given phase Φ_i may be written as

$$r(\chi) = \frac{\Phi_i}{k_i(\theta)\cos(\theta - \chi)}, \tag{36}$$

in which θ may be regarded as a generating parameter for χ through (34), which shows that the ray direction χ is perpendicular to the wave number diagram at a given θ. The curve given by (36) is therefore the reciprocal polar of the wave number curve and lends itself to the geometrical interpretation shown in figure 1 in which OP represents the wave number vector and OQ is the radius vector of the reciprocal polar to the curve (see also Lighthill 1978, p. 372-373).

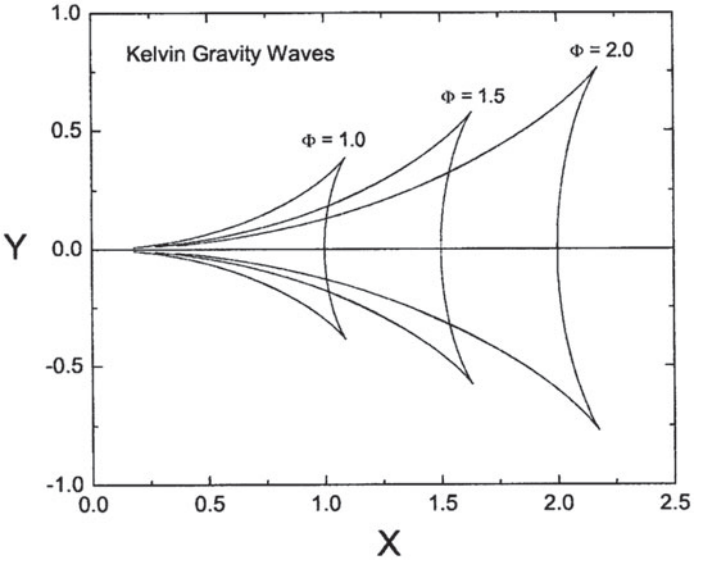

Figure 2. The family of deltoids (reciprocal polars) for the classic ship wave pattern. The semi-angle of the Kelvin wedge is $\sin^{-1}(1/3) \sim 19.5°$) and arises from the point of inflection of the wave number curve.

This particular figure is, in fact, appropriate to the stationary wave number diagram for surface gravity waves generated by a uniformly moving source, and gives rise to the deltoid shape characteristic of the classic ship wave pattern exhibiting a Kelvin-wedge cusp associated with the point of inflection of the wave number curve (as shown in figure 2).

4.2. *Rossby radiation pattern in a zonal wind*

Here, we extend the work of McKenzie (under review) on the radiation pattern of Rossby waves to include the effects of winds or flows. In the case of a constant zonal flow $U\hat{\boldsymbol{x}}$ the Rossby wave dispersion relation (27) becomes

$$k^2 + f^2/c^2 = \frac{-\beta k \cos\theta}{(\omega - Uk\cos\theta)}, \tag{37}$$

which is a cubic for $k(\theta)$. In the classic case of $f^2/c^2 = 0$ (corresponding to infinite Rossby radius) this equation reduces to a quadratic with solutions

$$k_{\pm}(\theta) = \frac{\omega}{2U\cos\theta}\left(1 \pm \sqrt{1 + 4M_r\cos^2\theta}\right), \qquad M_r \equiv \beta U/\omega^2. \tag{38a,b}$$

M_r is a "Rossby" Mach number measuring the flow speed in units of the speed ω^2/β characteristic of the Rossby zonal wave speed. At mid-latitudes this speed ranges from $80\,\mathrm{ms}^{-1}$ for two day wave periods to $20\,\mathrm{ms}^{-1}$ for four day periods. Therefore, M_r may take a wide range of values from the very small to of the order of or greater than unity depending upon the wind speed and the wave period.

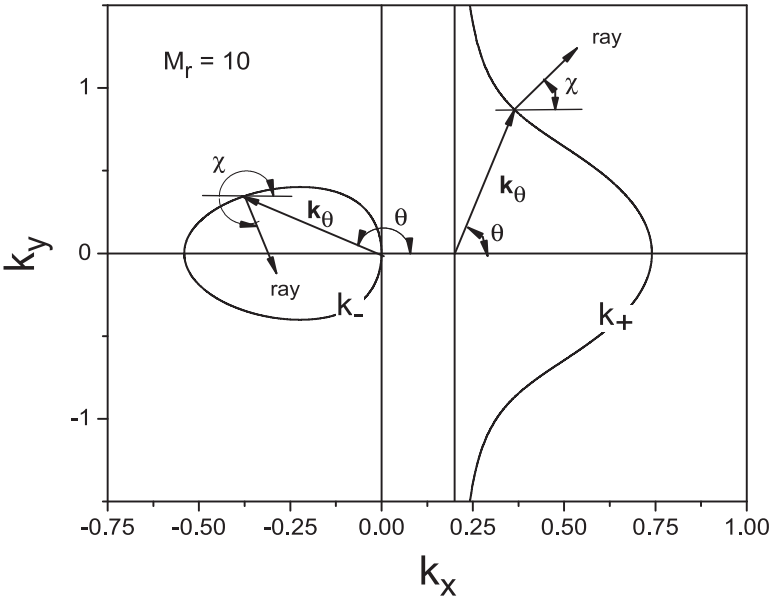

Figure 3. The wave number curves $k_{\pm}(\theta)$ for Rossby waves in a westerly zonal wind ($U > 0$), illustrating the relation between the ray direction χ and the wave number angle θ for each curve.

4.2.1. *Westerly wind*

In the case of a westerly wind ($U > 0$, $M_r = 10$), the wave number curves given by (38a) are shown in figure 3.

The $k_{-}(\theta)$ is the closed ovoid-like curve lying in $k_x < 0$ (corresponding to westward phase propagation) modified slightly by the flow so that it extends to $k_x = k_{-}(\theta = \pi)$ rather than $-\beta/\omega$, whereas the $k_{+}(\theta)$ is a new mode arising from the zonal flow, consisting of the line $k_x = \omega/U$ with the forward facing indentation at $k_x = k_{+}(\theta = 0)$.

The relation between the ray angle χ and the wave number angle θ follows from (35) in which we use (38a) for $k(\theta)$ yielding

$$k'(\theta) = \frac{\omega}{2U}\frac{\sin\theta}{\cos^2\theta}\,(A \pm 1)\,, \tag{39}$$

and hence

$$\tan\chi = \frac{t\,(1 \mp 1/A)}{\left(1 \pm t^2/A\right)}, \qquad t \equiv \tan\theta \tag{40a,b}$$

with

$$A = \sqrt{1 + 4M_r\cos^2\theta}. \tag{40c}$$

The variation of χ for $k_{\pm}(\theta)$ wave number curves at $M_r > 1$ are shown in figures 4(a),(b). The $k_{\pm}(\theta)$ curves for various M_r are shown in figure 5.

The radiation pattern for the closed Rossby wave normal diagram $k_{-}(\theta)$ yields a family of parabolic like curves as shown in figure 6(a) for the case $M_r = 10$. These are similar to the case of no flow (Rhines 2003, McKenzie under review), which consists of two families of hyperbolas, these being the reciprocal polars of the Longuet-Higgins offset circle. On the other

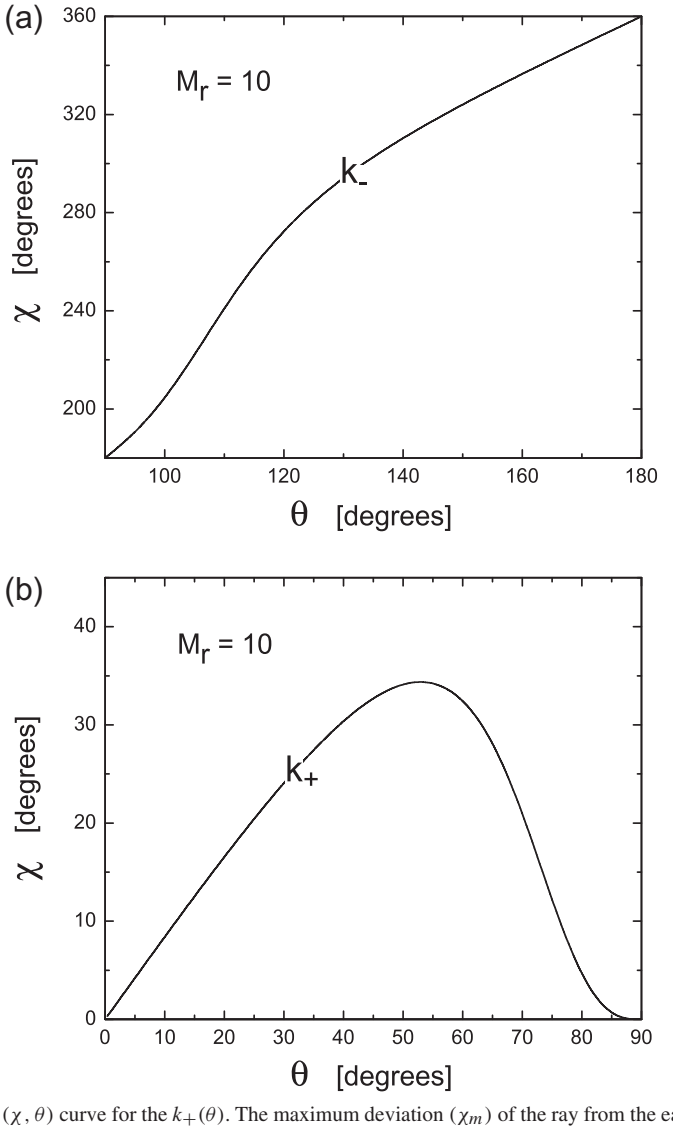

Figure 4. (a) The (χ, θ) curve for the $k_+(\theta)$. The maximum deviation (χ_m) of the ray from the east arises from the point of inflection in the $k_+(\theta)$. Note $\exists$ two values of θ for any given $\chi(<\chi_m)$. (b) The (χ, θ) curve for the $k_-(\theta)$ wave number curve.

hand the reciprocal polar of the westward branch $(k_+(\theta))$, namely the "indented line", yields the radiation pattern as the family of deltoid-like curves shown in figure 6(b) for $M_r = 10$.

These curves resemble a "reverse" ship wave with the disturbance confined to a Kelvin-like wedge angle which is given by the ray direction at the point of inflection of the $k_+(\theta)$ in figure 3. To a good approximation this critical wedge-angle χ_I is given by

$$\tan \chi_I = \left(\frac{3}{4}\right)^{3/2} \frac{\left(\sqrt{1+4M_r}-1\right)}{2}, \tag{41}$$

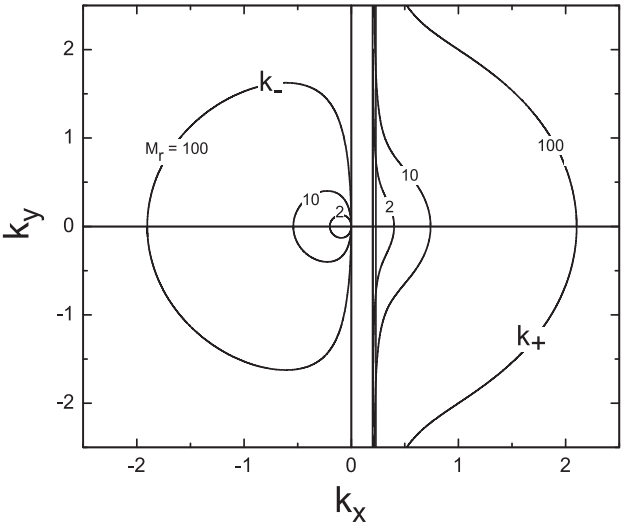

Figure 5. The $k_{+,-}(\theta)$ wave number curves for various values of M_r.

which shows that $\chi_I \to 0$ as $M_r \to 0$, $\chi_\pm \simeq 22°$ for $M_r = 1$, and $\chi_- \to 90°$ as $M_r \to \infty$. The "reversed" ship wave pattern (figure 6(b) arises from the shape of the $k_+(\theta)$ (figure 3) exhibiting the indentation to the right (i.e. $k(\theta)\cos\theta$ increases with θ).

4.2.2. *Easterly wind*

For $U < 0$ the wave number curves, for various values of $M_r < 0$ are shown in figure 7.

The open branch with the asymptote $k_x = \omega/U$ and the indentation at $k_x = k_+(\theta = \pi)$ now lie entirely westward ($k_x < 0$). We note that as $M_r \to -1/4$ the open and closed branches coalesce and for $|M_r| > 1/4$ are joined as shown in figure 7 for $M_r = -0.3$ and -0.275. The associated radiation patterns are shown in figures 8 and 9.

In figure 8, we observe that the family of deltoids lie entirely to the west (in the direction of the wind) and, in contrast to the case of a westerly, the deltoids face the same way as would a Kelvin ship wave. This is because in the corresponding wave number curves (labeled $M_r = -0.225$), the line with the indentation lies to the right of the asymptote (i.e. to the west). In the latter, the deltoid "interacts" with the parabolic-like curves.

4.2.3. *Stationary wave*

For the case of stationary waves in the laboratory frame, in which we let $\omega = 0$ and consider the case $f^2/c^2 \neq 0$ so that equation (37) becomes

$$k^2 = (\beta/U) - (f^2/c^2), \qquad k_x = 0. \tag{42a,b}$$

Hence, the wave normal diagram becomes a circle of radius $\sqrt{(\beta/U) - (f^2/c^2)}$ if U is westerly and less than $\beta c^2/f^2$, which is the long wavelength zonal phase speed of the Rossby wave, but is otherwise evanescent when $U < 0$. However, the line $k_x = 0$ is also part of the wave number diagram, whose complete form is shown in figure 10(a).

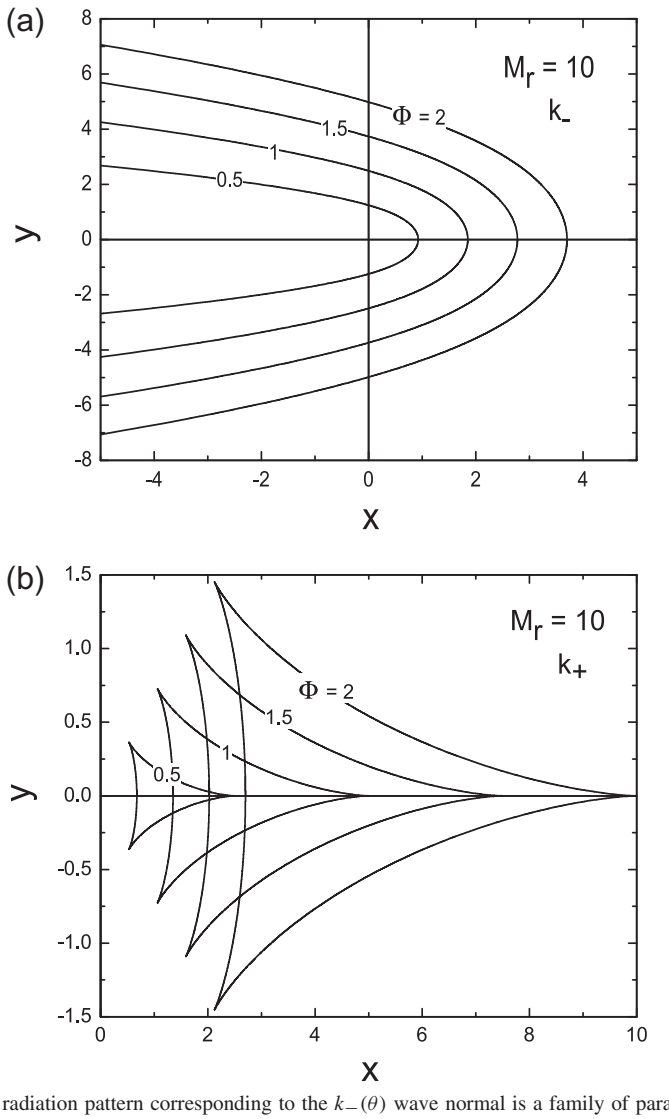

Figure 6. (a) The radiation pattern corresponding to the $k_-(\theta)$ wave normal is a family of parabolic-like curves, which is reminiscent of the capillary waves generated by an object in a stream. (b) The radiation pattern (family of reciprocal polars- deltoids) for the $k_+(\theta)$ wave number for $M_r = 10$. The pattern looks like an "reversed" ship wave pattern. The cusps result from the point of inflection in the $k_+(\theta)$ curve and confine the pattern to a semi-wedge angle χ_m.

The direction of the arrows (rays) are obtained from the limiting form of the general wave normal diagram as $\omega \to 0$ ($M_r \to \infty$) as shown in figure 5. This case is similar to the two-dimensional internal gravity wave pattern generated in a horizontal flow (Lighthill 1978 p. 415, 416 figures 108(a),(b)). The reciprocal polar is shown in figure 10(b) and consists of the semi-circle (taken twice), the double line $k_y = 0$ (for $k_x >$ radius of circle) and the two lines extending westwards.

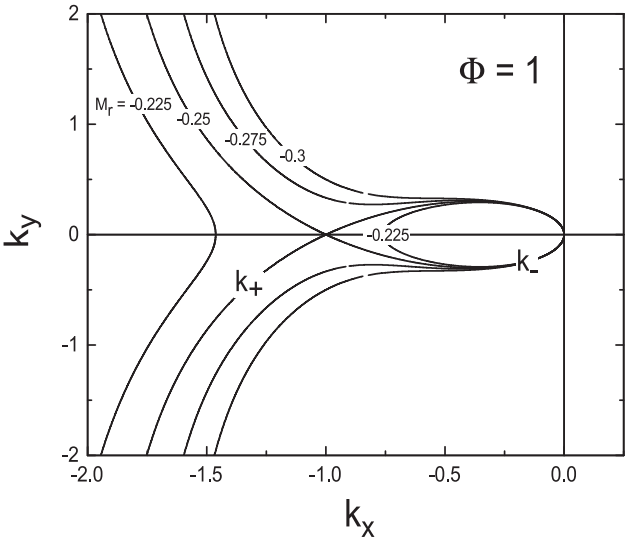

Figure 7. The $k_{+,-}(\theta)$ curves in an easterly wind ($U < 0$) for various values of M_r. For $|M_r| > 1/4$ the curves coalesce as shown.

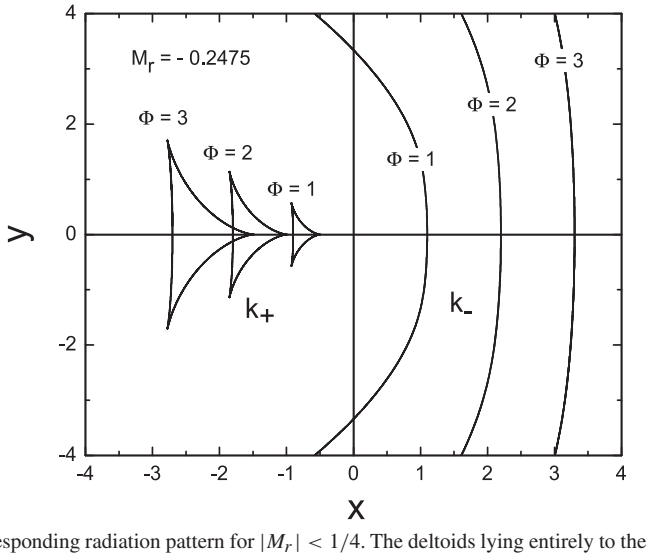

Figure 8. The corresponding radiation pattern for $|M_r| < 1/4$. The deltoids lying entirely to the west correspond to the open branch (plane with an indented line), whereas the parabolic like curves are associated with the closed ovoid, and lie both ahead (east) and behind (west).

4.3. *Radiation patterns in a meridional wind*

In the case of a constant meridional wind/flow, $U\hat{\boldsymbol{y}}$, the Rossby wave dispersion relation (27) becomes

$$k^2 + f^2/c^2 = -\frac{\beta k \cos\theta}{\omega - kU\sin\theta}. \tag{43}$$

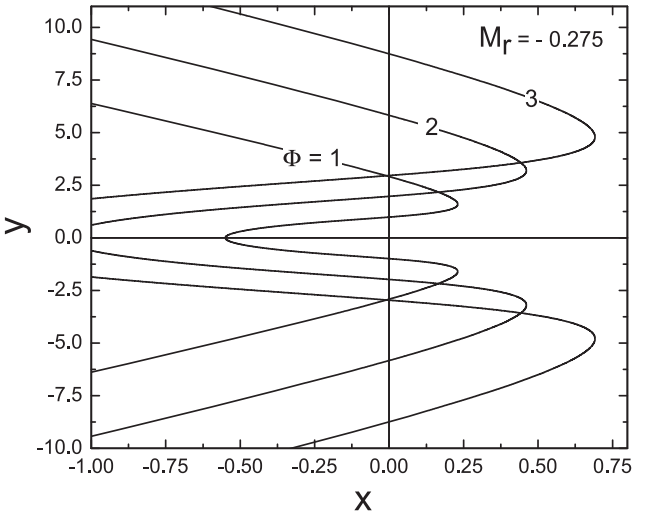

Figure 9. The radiation pattern, for $|M_r| > 1/4$ and various Φ, which involves an "interaction" between the deltoids and paraboloids.

We consider the classic case $c \to \infty$ (but return to c finite in the case of stationary waves, given at the end of this section). Equation (43) becomes a quadratic for $k(\theta)$ with solutions (after factoring out $k = 0$)

$$k_\pm = \frac{\omega}{2U \sin\theta}\left(1 \pm \sqrt{1 + 4M_r \sin\theta \cos\theta}\right). \tag{44}$$

The $k_+(\theta)$ and $k_-(\theta)$ wave number curves for various M_r are shown in figure 11. Note that for ($M_r > 1/2$) the open and closed curves (for k_+ and k_-, respectively) coalesce.

The radiation patterns (reciprocal polars) are calculated using equations (36) with (35) and the wave number curves $k_\pm(\theta)$ given by (44). We obtain from (35) and (44) the relation between the ray angle χ and the wave number angle θ:

$$\tan\chi = \tan\theta\left(1 \pm \frac{B}{A\tan^2\theta}\right)\Big/\left(1 \mp \frac{B}{\tan^2\theta}\right) \tag{45a}$$

with

$$A \equiv \sqrt{1 + 2M_r \sin 2\theta}, \qquad B \equiv (1 + 2M_r \tan\theta)/(1 \pm A)\,. \tag{45b,c}$$

The corresponding radiation patterns for $M_r \le 0.5$ are shown in figure 12 (for $k_+(\theta)$) and figure 13 (for $k_-(\theta)$). The cusps in the radiation pattern shown in figure 12 arise from the points of inflection in the wave number curve $k_+(\theta)$ for $M_r = 0.4$.

In the case of $M_r > 1/2$, the open and closed curves "interact", or coalesce, as already noted and illustrated in figure 11. The reciprocal polars for $M_r = 0.45$, 0.5, and 0.55 are shown in figure 14. In this case, the $k(\theta)$ curve given by (44) is complex in the angular range $\theta_- > \theta > \theta_+$, where

$$\sin\theta_\pm = \sqrt{\frac{1 \pm \sqrt{1 - (1/4)M_r^2}}{2}}. \tag{46}$$

The angles $\theta_{+,-}$ lie in the second quadrant.

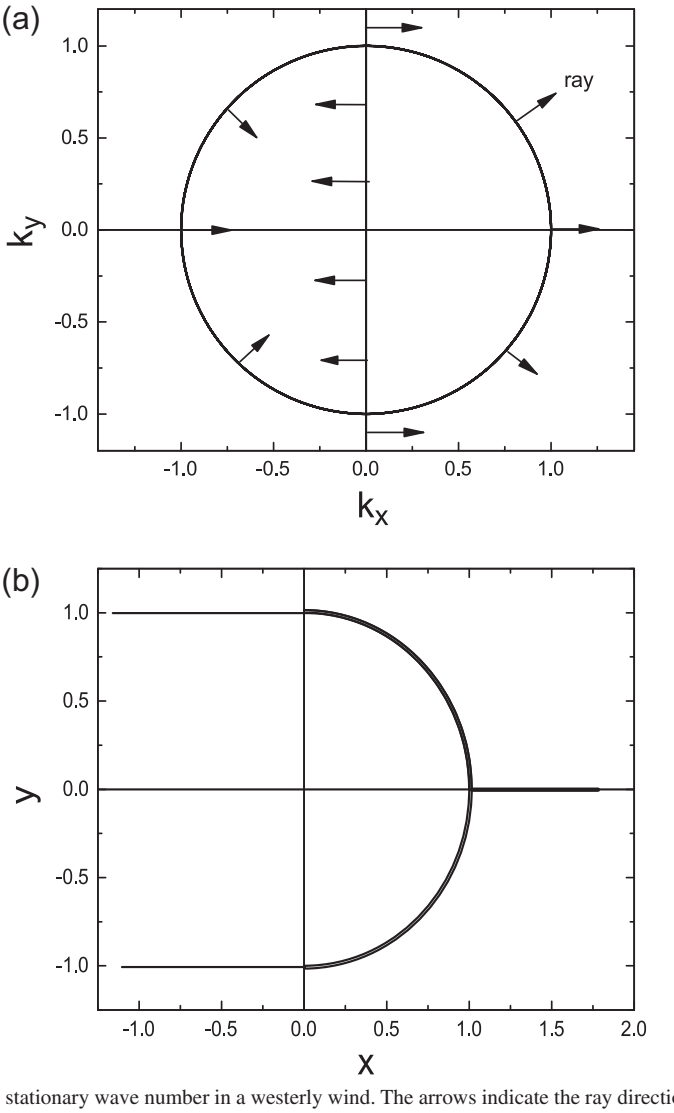

Figure 10. (a) The stationary wave number in a westerly wind. The arrows indicate the ray directions which can be deduced from figure 6 for the case of $M_r = 100$ (ω small). (b) The corresponding reciprocal polar.

In the case of stationary waves ($\omega = 0$), the dispersion equation becomes

$$k^2 = \frac{\beta}{U}\cot\theta - \frac{f^2}{c^2} = \frac{\beta}{U}\left(\cot\theta - \cot\theta_c\right), \tag{47}$$

where

$$\cot\theta_c = \frac{U}{\beta}\frac{c^2}{f^2}. \tag{48}$$

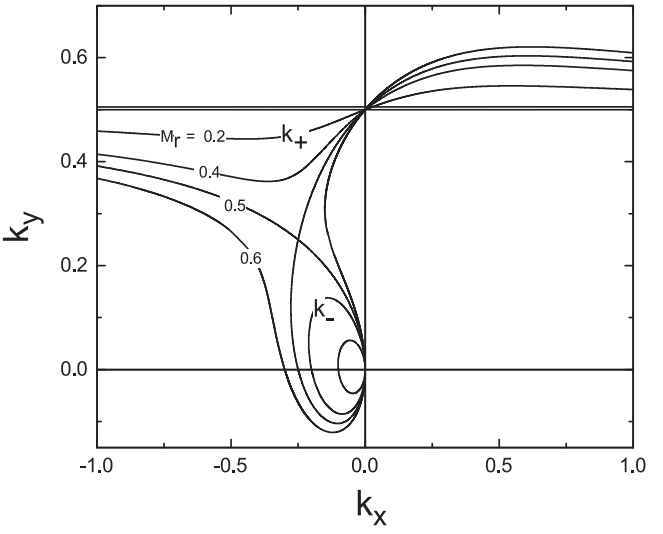

Figure 11. The wave number curves $k_+(\theta)$ and $k_-(\theta)$ in a meridional wind for various values of M_r. The curves coalesce for $M_r \geq 1/2$.

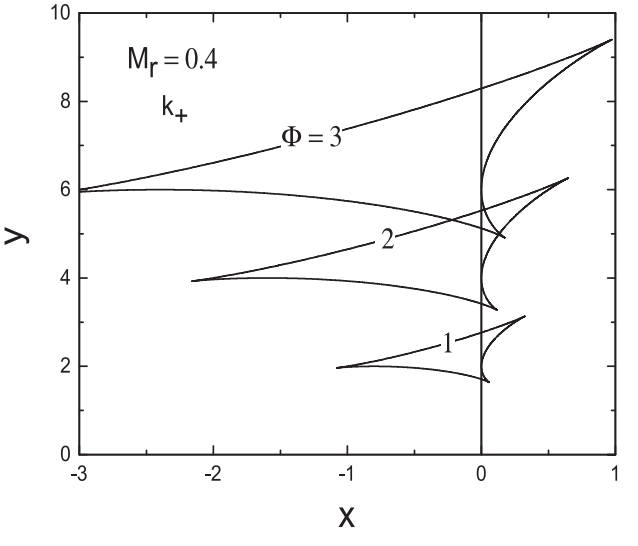

Figure 12. The radiation pattern for the wave number $k_+(\theta)$ for various Φ with $M_r = 0.4$.

cot θ_c is therefore another Rossby "Mach" number where the flow speed is measured in units of the long wavelength Rossby speed which, at mid-latitudes, takes values from about 120 ms^{-1} in an ocean of depth 4 km to around 200 ms^{-1} in the atmosphere.

The wave number diagrams and their associated reciprocal polars are shown, respectively, in figures 15 and 16 for various values of θ_c. The radiation patterns for various Φ are shown in figure 17 for the case $\theta_c = 90°$.

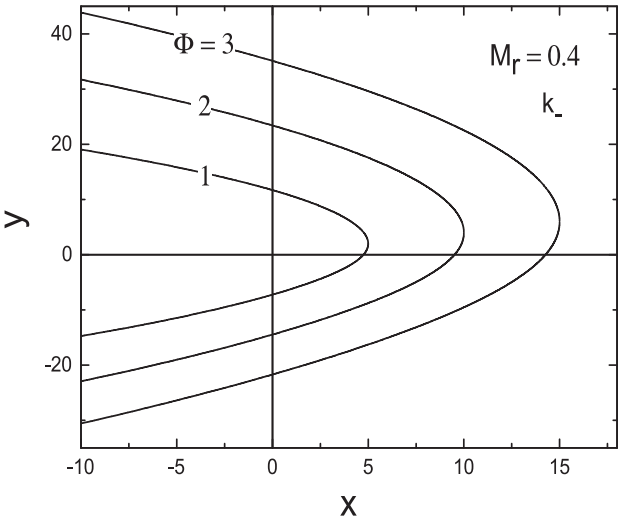

Figure 13. The radiation pattern for $k_{-}(\theta)$ wave number for various Φ at $M_r = 0.4$, exhibiting the parabolic-type curves similar to capillary waves.

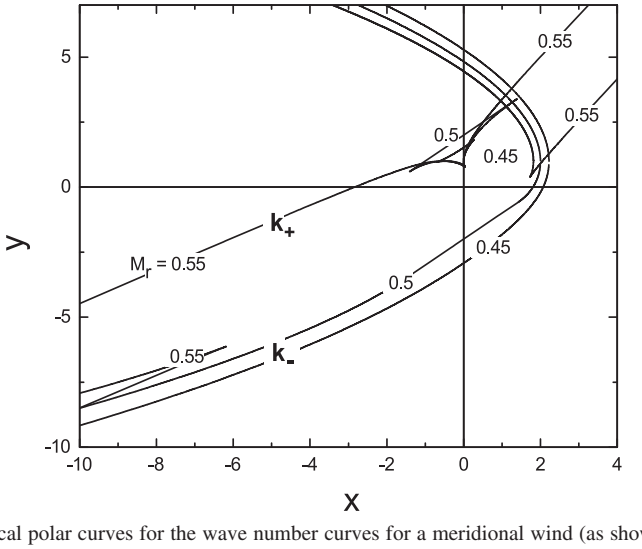

Figure 14. Reciprocal polar curves for the wave number curves for a meridional wind (as shown in figure 11) for $M_r = 0.45, 0.5$, and 0.55. Note the two "Mach"-like lines, which appear for $M_r = 0.55$ on the k-curve, and which are associated, in the wave number curves of figure 11, with the asymptote tangent lines drawn from k_x, k_y origin to the two points where the rays are normal to the wave number curve.

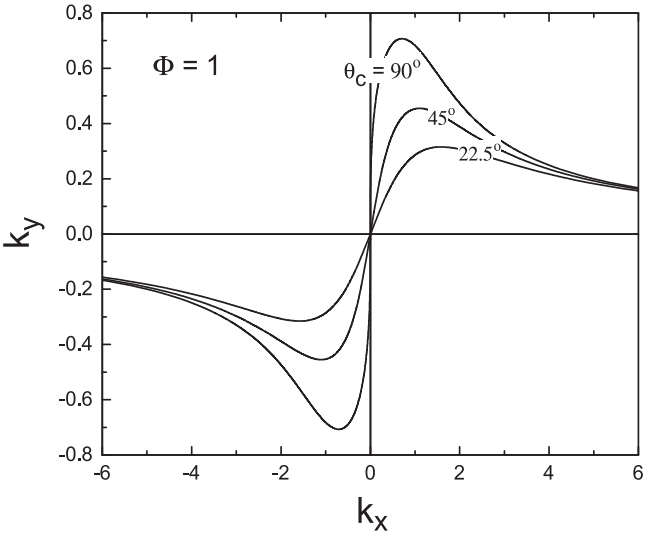

Figure 15. Stationary wave number curve in meridional wind for various θ_c.

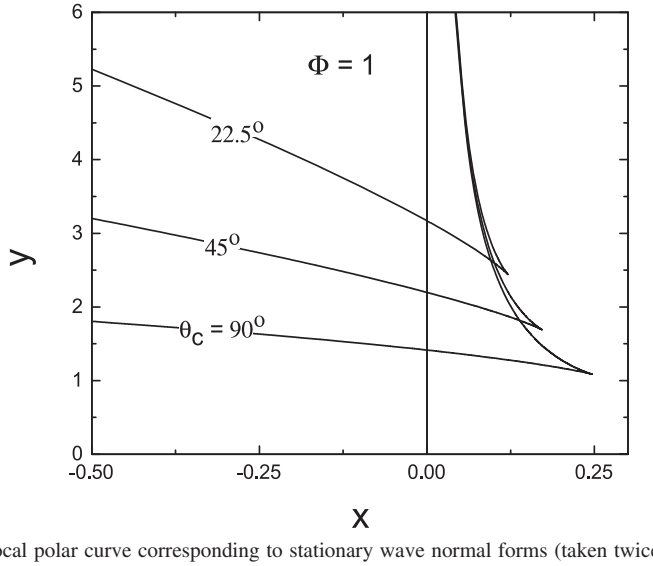

Figure 16. Reciprocal polar curve corresponding to stationary wave normal forms (taken twice) for a meridional wind (figure 15).

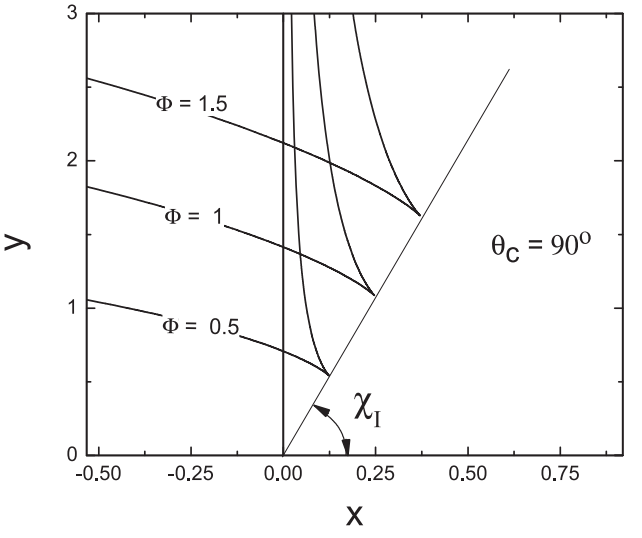

Figure 17. The stationary radiation pattern in a meridional wind.

5. Summary

For Fourier type zonal plane wave modes, we derive a second-order differential equation describing the latitudinal structure of Rossby type wave perturbations on a β-plane in zonal (and meridional) winds.

We have followed Lighthill (1978) to show how the local dispersion equation, when interpreted as a wave number diagram in $\boldsymbol{k}$ space at a given frequency ω, can be used to construct the radiation pattern generated by a time harmonic compact source in a laboratory frame relative to which zonal and meridional winds flow/blow. The effect of the Doppler shift in frequency, due to the mean flow, on the wave number curve (the Longuet-Higgins offset circle in the rest frame) is quite dramatic and is highlighted by a series of figures 3–8. The most important effect is the appearance of a new branch in $\boldsymbol{k}$-space caused by the background wind consisting of a blocking line with an indentation. In the case of a zonal wind, the new branch consists essentially of the line ($k_x = \omega/U$) with the indentation facing to the right. In the case of a westerly flow, the radiation pattern associated with this branch is a family of deltoids which resemble a reverse ship wave pattern (see figure 6(b)). On the other hand, the radiation pattern associated with the distorted Longuet-Higgins circle is a family of parabolic-like curves rather similar to the wind-free case (e.g. see figure 6(a)). In the case of a westward wind (an easterly flow), the radiation pattern is shown in figure 8 with the family of deltoids lying entirely to the west and embedded in the parabolic like patterns associated with the closed wave number curve. However, if $|M_r| > 1/4$ an interaction between the deltoids and the parabolic curves as depicted in figure 9 arises. The case of a meridional wind is slightly more complicated but again these diagrams (figures 11–17) depict the diversity of the radiation patterns. In the case of stationary waves in the laboratory frame, we obtain the interesting figures 12 and 14 for the zonal and meridional cases, respectively. The new results here have the wave number curves in zonal and meridional flows and their reciprocal polars which provide the various Rossby

radiation patterns. These provide the Rossby wave problem equivalent to the classic ship wave problem (involving both gravity and capillary waves) and internal gravity waves in a wind.

Acknowledgements

The authors wish to thank the National Research Foundation of South Africa and TBD (Under NRF grant number: 2053776) for support and express a heartfelt appreciation for the most useful and constructive work of the anonymous reviewers toward the finalization of this paper.

References

Booker, J.R. and Bretherton, F.P., The critical layer for internal gravity waves in a shear flow. *J. Fluid Mech.* 1967, **27**, 513–539.

Bretherton, F.P. and Garrett, C.J.R., Wave trains in inhomogeneous moving media. *Proc. R. Soc. Lond. A* 1968, **302**, 529–554.

Dickinson, R.E., Planetary Rossby waves propagating vertically through weak westerly wind wave guides. *J. Atmos. Sci.* 1968, **25**, 984–1002.

Doyle, T.B. and McKenzie, J.F., Stationary wave patterns in deep water. *Quest. Math.* 2013, **36**, 1–14.

Duba, C.T. and McKenzie, J.F., Propagation properties of Rossby waves for latitudinal β-plane variations of f and zonal variations of the shallow water speed. *Ann. Geophys.* 2012, **30**, 1–7.

Eckart, C., *Hydrodynamics of Oceans and Atmospheres*, 1960 (Cambridge: Pergamon Press).

Eltayeb, A. and McKenzie, J.F., Propagation of hydromagnetic planetary waves on a beta-plane through magnetic and velocity shear. *J. Fluid Mech.* 1977, **81**, 1–12.

Gerkema, T., Maas, L.R.M. and van Haren, H., A note on the role of mean flows in Doppler-shifted frequencies. *J. Phys. Oceanogr.* 2013, **43**, 432–441.

Gill, A.E., *Atmosphere and Ocean Dynamics*, 1982 (London: Academic Press).

Lighthill, J., Studies on magneto-hydrodynamical waves and their anisotropic wave motions. *Proc. R. Soc. Lond. A* 1960, **252**, 397–430.

Lighthill, J., *Waves in Fluids*, 1978 (Cambridge: Cambridge University Press).

Longuet-Higgins, M.S., Planetary waves on a rotating sphere. *Proc. R. Soc. Lond. A* 1964, **279**, 446–473.

McKenzie, J.F., The group velocity and radiation patterns of Rossby waves. Sub judice 2013.

Mekki, O.M. and McKenzie, J.F., The propagation of atmospheric Rossby-gravity waves in latitudinally sheared zonal flows. *Phil. Trans. R. Soc. Lond. A* 1977, **287**, 115–143.

Pedlosky, J., *Geophysical Fluid Dynamics*, 1987 (New York: Springer-Verlag).

Ratcliffe, C., *An Introduction to the Ionosphere and Magnetosphere*, 1972 (Cambridge: Cambridge University Press).

Rhines, P.B., Rossby waves. In *Encyclopaedia of Atmospheric Sciences*, edited by J.R. Holton, J.A. Curry and J.A. Pyle, pp. 1–37, 2003 (Academic Press: Oxford).

Vallis, G., *Atmospheric and Oceanic Fluid Dynamics: Fundamentals and Large-scale Circulation*, 2006 (Cambridge: Cambridge University Press).